Organic & Biomolecular Chemistry

Cite this: *Org. Biomol. Chem.*, 2012, **10**, 6341

www.rsc.org/obc

PAPER

Cross-docking study on InhA inhibitors: a combination of Autodock Vina and PM6-DH2 simulations to retrieve bio-active conformations†

Jean-Luc Stigliani,*[a,b] Vania Bernardes-Génisson,*[a,b] Jean Bernadou[a,b] and Geneviève Pratviel[a,b]

Received 22nd March 2012, Accepted 8th June 2012
DOI: 10.1039/c2ob25602a

InhA, the NADH-dependent enoyl-acyl carrier protein reductase from *Mycobacterium tuberculosis* (Mtb) is the proposed main target of the first-line antituberculosis drug isoniazid (INH). INH activity is dependent on activation by the catalase peroxidase KatG, a Mtb enzyme whose mutations are linked to clinical resistance to INH. Other inhibitors of InhA that do not require any preliminary activation are known. The design of such direct potent inhibitors represents a promising approach to circumvent this resistance mechanism. An ensemble-docking process with four known InhA X-ray crystal structures and employing the Autodock Vina software was performed. Five InhA inhibitors whose bioactive conformations are known were sequentially docked in the substrate cavity of each protein. The efficiency of the docking was assessed and validated by comparing the calculated conformations to the crystallographic structures. For a same inhibitor, the docking results differed from one InhA conformation to another; however, docking poses that matched correctly or were very close to the expected bioactive conformations could be identified. The expected conformations were not systematically well ranked by the Autodock Vina scoring function. A post-docking optimization was carried out on all the docked conformations with the AMMP force field implemented on the VEGAZZ software, followed by a single point calculation of the interaction energy, using the MOPAC PM6-DH2 semi-empirical quantum chemistry method. The conformations were subsequently submitted to a PM6-DH2 optimization in partially flexible cavities. The resulting interaction energies combined with the multiple receptor conformations approach allowed us to retrieve the bioactive conformation of each ligand.

Introduction

Mycobacterium tuberculosis (Mtb), the etiologic agent of tuberculosis, produces long fatty acids (C18 to C30) precursors of mycolic acids, which are involved in the cell wall biosynthesis, *via* a type II fatty acid elongation system (FAS-II).[1] This system includes the reduction of a *trans* double bond conjugated to the carbonyl group of fatty acyl substrates, catalyzed by InhA, an NADH-dependent enoyl-acyl carrier protein reductase (enoyl-ACP reductase).[2,3] InhA is considered as the major target for isoniazid (INH, isonicotinic acid hydrazide),[4] one of the oldest synthetic and the most prescribed drug for the treatment of tuberculosis.[5] INH is a pro-drug that must be activated by the mycobacterial catalase-peroxidase enzyme KatG;[6,7] the activated form of INH then binds covalently to the nicotinamide ring of NADH. The resulting INH-NADH adduct has been shown to be a competitive inhibitor of wild-type InhA of Mtb.[8–11]

Triclosan (TCL), a broad spectrum antimicrobial agent,[12–15] has been found to inhibit InhA in Mtb and *M. smegmatis*.[16] Binding of TCL to wild-type InhA was shown to be uncompetitive with respect to NADH.[17] Structural data[18,19] showed that TCL occupied the acyl substrate-binding pocket and was therefore in a separate region from the site of INH-NADH adduct binding. Structure-based drug design[19,20] and high-throughput screening programs[18,21,22] have been performed in an attempt to develop new inhibitors. These compounds are alkyl diphenyl ethers TCL analogues,[19,20] arylamide series compounds,[21] pyrrolidine carboxamides[22] or indole-5-amides.[18] All these compounds interact with InhA in similar way as TCL, *i.e.* by non-covalent binding in the substrate-binding site. In contrast to INH, they do not require a preliminary activation by the mycobacterial KatG enzyme and are effective against wild-type and drug-resistant strains of Mtb.[18–20] Therefore, the acyl substrate-binding pocket is a promising target for the development of new antitubercular agents.

During the past decade, our interest in InhA led us to design small molecules inspired by the INH-NADH adducts.[23–25] Some

[a]*CNRS, LCC (Laboratoire de Chimie de Coordination), 205 route de Narbonne, BP 44099, F-31077 Toulouse Cedex 4, France. E-mail: stigliani@lcc-toulouse.fr*
[b]*Université de Toulouse, UPS, INPT, F-31077 Toulouse Cedex 4, France*
†Electronic supplementary information (ESI) available. See DOI: 10.1039/c2ob25602a

of these molecules displayed significant inhibitory activities towards InhA enzyme and mycobacterial growth.[26] In order to gain insight regarding their mode of binding in the active site of InhA and to further develop optimized inhibitors, we planned to perform docking studies. Protein flexibility represents an important aspect in docking methodology. Although modern programs can take into consideration the side chain flexibility, direct modeling of the backbone movements remains an issue.[27,28] Several approaches to incorporate the flexibility of protein binding sites have been described.[27,29–32] In the multiple receptor conformations approach, the flexibility of the receptor is considered using several crystallographic structures of the same protein.[33,34] With a representative set of protein structures in complex with ligands, large conformational changes such as backbone rearrangements can be taken into account.

In the present work, the multiple receptor conformations approach was used to develop and validate a docking methodology, using a set of four InhA structures and five InhA inhibitors for which crystallographic data are available. Each inhibitor was sequentially docked into the different selected InhA structures (cross-docking procedure) with the Autodock Vina software.[35]

All of the resulting docking poses were then energy-minimized into their binding pocket using molecular mechanics force-field. Finally, an interaction energy calculation was applied to each protein–ligand complex, using the semi-empirical quantum chemistry PM6-DH2 method.[36,37] This value appeared very efficient to locate the bioactive conformations among the whole of the docking results and was shown to improve the ranking obtained with Autodock Vina.

The aim of this work is to develop a performant docking approach to gain more insight regarding the mode of binding of new direct InhA inhibitors. This approach will subsequently be used in the screening and the design of new potential InhA inhibitors.[38]

Materials and methods

Proteins and ligands

The crystallographic structures of InhA (or *E. coli* FabI in one case) in complex with inhibitors were taken from the Brookhaven Protein Data Bank.[39] A large number of 3D structures of InhA co-crystallized with numerous inhibitors can be found. However, some of these belong to the same chemical families and are very similar. Hence, we selected a representative inhibitor for each of these families. For convenience, the ligand abbreviation found in the PDB files is used (Table 1). The related PDB entry codes were **1P44**, **1P45**,[18] **2H7M**[22] and **3FNE**.[20] In the **1P45** structure, two TCL molecules fill the substrate-binding pocket.[18] The phenol ring of the first one undergoes a stacking interaction with the nicotinamide ring of the cofactor and both the TCL phenolic and ether oxygens participate in hydrogen-bonding interactions involving the conserved Y158 and the 2′-hydroxyl of the nicotinamide ribose of the cofactor in the catalytic active site. The second TCL molecule exhibits an inverted orientation relative to the first one and resides in an almost entirely hydrophobic area within the substrate binding cavity. The wide volume of the binding pocket

Table 1 The selected InhA and FabI proteins with their respective inhibitors[a]

PDB entry	Inhibitor	Structure	InhA IC_{50} (μM)[b]
1P45	TCL	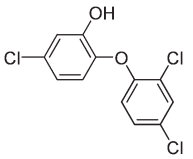	1.10[20]
1P44	**GEQ**	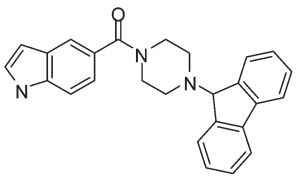	0.16[18]
2H7M	**d11**	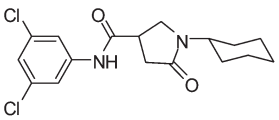	0.39[22]
3FNE	**8PC**	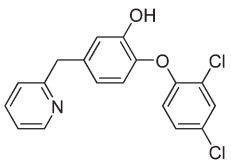	0.029[20]
2B37	**8PS**	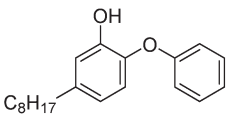	0.005[19]
1LXC[c]	**AYM**	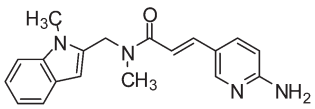	0.37[d] [40]

[a] Only proteins and inhibitors highlighted in bold were the subject of this study. [b] Concentration of inhibitor that reduces the enzymatic activity by 50%. [c] Enoyl-ACP reductase of *E. coli* (FabI). [d] On *E. coli* FabI.

generated by this double occupation seemed propitious to docking assays. TCL itself was not incorporated in the study. The inhibitor found in **1P44** is a 1-(fluorenyl)-4-(indolylcarbonyl)piperazine derivative referred to as **GEQ**. This bulky compound fills the volume occupied by the natural substrate. In **2H7M**, one finds a cyclohexyl-pyrrolidinone carboxamide substituted by a dichlorophenyl group (**d11**) and in **3FNE**, a TCL derivative substituted by a pyridinyl methylene group (**8PC**). The inhibitors **GEQ**, **d11** and **8PC** were used in this study. The alkyl diphenyl ether **8PS**, a TCL analogue which was co-crystallized with InhA and found in the PDB entry **2B37**,[19] was also included in the series because of the presence of the C_8 alkyl chain which extends into the hydrophobic region of the substrate binding cavity. As the InhA structure found in **2B37** was not totally resolved (the L197-G204 amino acid chain which surrounds the binding pocket is missing), this protein was not considered in the docking process. Finally we added the aminopyridine derivative **AYM** known to interact with the enoyl-ACP reductase FabI (homologue of InhA in *E. coli*, PDB code **1LXC**[40]) that exhibits a good *in vitro* antibacterial activity against several germs. The amino acid sequence of FabI which

slightly differs from the InhA one and was not used as receptor. Thus, five inhibitors were docked into four InhA structures (Table 1).

The ligands and water molecules were extracted from the PDB files. The MolProbity software[41] was used to assign the position of hydrogen atoms and the protonation state of histidines. NAD (H) cofactor was conserved into the co-crystallized InhA-inhibitor complexes. The nicotinamide is experimentally used under its oxidized (NAD^+) or reduced form (NADH) in the various co-crystallization processes. We choose to consider the NADH form in our calculations. Hydrogens were independently added on the crystal structure of nicotinamide cofactors and energy-minimized using the AMMP[42] force field implemented on the VEGA ZZ[43] molecular modeling package. The ligands of this study were thoroughly built and fully optimized before the docking stage. The partial atomic charges were computed with the PM6 Hamiltonian[36] implemented in the MOPAC2009 quantum chemistry package.[44]

Docking

All of the calculations were performed with the docking program Autodock Vina v1.1.[35] The choice of Autodock Vina as docking software was directed by its ability to find bioactive conformations with a very good level of accuracy and it was also found to retain a notable efficiency as the number of rotatable bonds increased.[45] Moreover, we could note its high speed in docking calculations. Finally, it was conceived to run on multi-CPU architectures.

The Autodock graphical interface AutoDockTools[46,47] was used to keep polar hydrogens and add partial charges to the proteins using the Kollman United charges. The search space was included in a box of 24 × 24 × 24 Å, centred on the binding site of the ligands and nicotinamide cofactor. The four selected proteins **1P44**, **1P45**, **2H7M** and **3FNE** of this study superimposed rather correctly as the computed RMSD was less than 0.7 Å. Moreover, a thorough analysis of the catalytic cavity showed that the nicotinamide cofactors were also well superimposable. However, distortions of the peptidic chain and displacement of some amino acid side chains induced by the ligands were noticed. Particularly, differences emerged in the side chain conformations of six residues, namely, M103, F149, Y158, M161, M199 and L218. These latter residues were allowed to rotate during the docking studies (15 torsions). Flexible torsions of side chains and ligands were assigned with Autotors, an auxiliary module of AutoDockTools. For each calculation, fifteen poses ranked according to the scoring-function of Autodock Vina were obtained. Several studies showed that a post-docking optimization, after a docking procedure could improve the docking results and the scoring.[31,48,49] Therefore, an energy refinement of all the docked conformations was carried out using the VEGAZZ software. The receptors were kept rigid while the ligands were energy-minimized with the AMMP force field.

Conception of a partially flexible model receptor and computation of the binding affinity with MOPAC2009

For each protein, amino acid residues centred on the binding site of the ligand and included in a sphere with a radius of 13 Å were selected. All the other residues were discarded. The valences of broken bonds were completed with hydrogen atoms. The resulting systems contained 70 residues or 1180 atoms, including the cofactor. The global charge of NADH was set to −2, considering that the two phosphate groups were deprotonated. In a previous work, we showed the good potentiality of semi-empirical methods (AM1 or PM3) to estimate the interaction enthalpies.[50] Here, energies were computed with the more recent PM6 Hamiltonian.[36] The localized molecular orbital method which was developed to enable calculation on large systems such as enzymes[51] and was implemented on MOPAC2009 (keyword MOZYME) was applied. The effects of the solvation interface were simulated with the continuum model COSMO[52] with a dielectric constant set to 78.4. In order to better describe the non-covalent interactions (*i.e.* dispersion and hydrogen-bonding interactions), the transferable H-bonding correction was added (PM6-DH2 method).[37,53] The interaction energies were calculated with the equation: $\Delta E = \Delta_f H$ (ligand–receptor complex) − $\Delta_f H$ (ligand alone) − $\Delta_f H$ (receptor alone). At first, the Vina/AMMP derived docking poses were merged into the cavities and the whole was submitted to a single point energy calculation. The complexes giving the lowest binding energies were then submitted to a PM6-DH2 minimization stage in which the ligand, a set of 12 residues delimiting the binding pocket (Table S1.† Online Resource) and the totality of hydrogen atoms were fully energy-minimized. The remaining residues were kept frozen. The gradient norm was set to 0.5 kcal mol^{-1} $Å^{-1}$. The visualization of the results, the RMSD calculations and the graphic illustrations were done with the Accelrys DS Visualizer v2.5 software.[54] For the clarity of the text, the optimization energies got from Autodock Vina, PM6-DH2 single point, PM6-DH2 optimization will be named E_{vina}, E_{sp}, E_{opt}, respectively.

Results

The purpose of this study was to estimate the efficiency of a multiple receptor conformations docking protocol in predicting the correct orientation of original inhibitors into the substrate binding cavity. In general, Autodock Vina proved able to find the bioactive structure of the studied ligands; but in several cases the orientation of some amino acid side chains impeded the inhibitors to properly position into the cavity. Consequently, the expected conformations were not necessarily well ranked by the Autodock Vina scoring function and the best ranked conformation was different from the expected crystallographic structure. Finally, the difference between two adjacent scores was small (*i.e.* 0.1–0.3 kcal mol^{-1}) and sometimes the energetic gap between the first and the last rank (for 15 models) did not exceed 2 kcal mol^{-1}. These observations led us to estimate the interaction enthalpies using the semi-empirical quantum mechanical PM6 method, which is considered to be more accurate than other similar methods.[36] Unlike molecular mechanics force fields, semi-empirical methods describe electronic and polarization effects. Non-covalent interactions such as dispersion energy and hydrogen-bonding are prevalent in macromolecules and are not modeled with sufficient accuracy with semi empirical quantum-chemical methods. For the purpose of better describing these interactions, we used the transferable H-bonding correction

term (PM6-DH2) which was found to improve the performance of PM6.[37,53] We noticed that the use of this functionality associated with the COSMO solvation model[52] allowed a better selection of the expected conformations in comparison with the *in vacuo* PM6 results (not shown).

The observation of available InhA/ligand crystal structures reveals that all the ligands interact with the enzyme in a similar way: a hydrogen-bonding network is found with the 2′-hydroxyl of the nicotinamide ribose of the cofactor and the hydroxyl group of the catalytic residue Y158. The importance of this hydrogen-bonding network was previously reported.[18,40] Thus, the existence of these H-bonds in the docked structures was taken into account to assess the accuracy of the calculations. Fig. 1 displays the H-bonds found with the inhibitors in their own crystallographic structure. In several cases, we noticed that the MOPAC energy-minimization improved the ligand positioning into the binding pocket; this was more particularly highlighted by the appearance of these critical H-bonds.

Finally, by superposing 14 InhA-inhibitors structures from the PDB (list of the PDB entries in Table S2,† Online Resource), we delineated a global volume including the suitable location of the inhibitors into the binding pocket. This volume was used to discard some poses according to their "out-of-cavity" location (Fig. 1f).

Each of the five ligands (**GEQ**, **d11**, **8PC**, **8PS**, **AYM**) was docked into the four InhA/NADH cavities (**1P44**, **1P45**, **2H7M**, **3FNE**), by using the flexible docking methodology. For each inhibitor and protein, the predicted binding energies of only the first Vina pose and of the most relevant model (*i.e.* the closest to the crystal conformation) are indicated in Table 2. The complete docking results are provided as Online Resource (Table S3†). The quality of the positioning was estimated by the heavy atom root-mean-squared deviation (RMSD) calculated between the Vina docked geometries and the crystallographic conformations of the corresponding ligands as reference. A RMSD value inferior or close to 2 Å was considered as a successful docking.

As expected, Autodock Vina could systematically find the correct conformation with the top-ranked pose in the self-docking procedures, *i.e.* when each ligand was individually docked into its native cavity (**GEQ**/**1P44**, **d11**/**2H7M**, **8PC**/

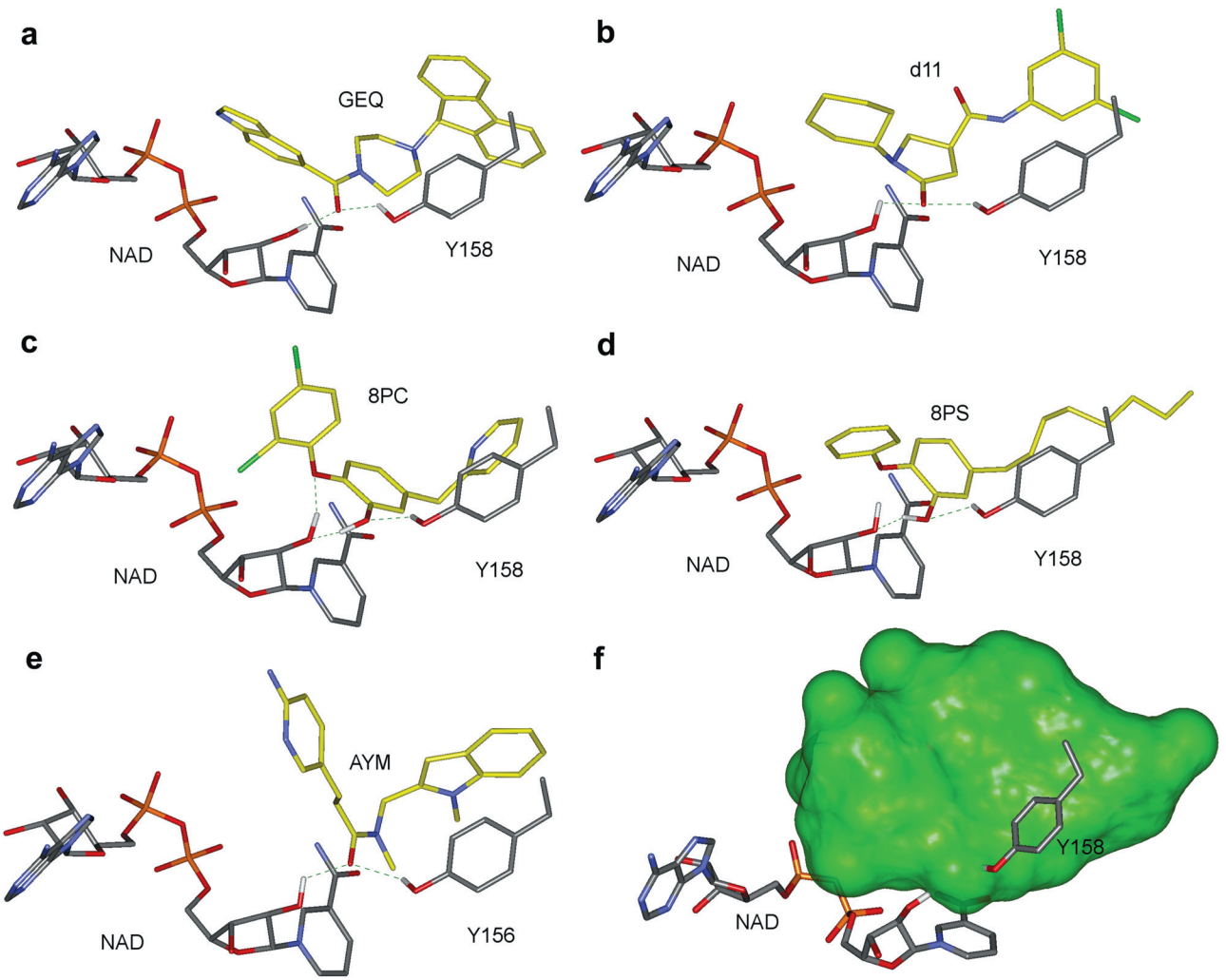

Fig. 1 Ligands of InhA in their crystal conformation. H-bonds between the ligands and Y158 as well as the 2′-hydroxyl nicotinamide ribose are indicated as green dotted lines. The ligands are found in the following PDB entries: (a) **1P44**,[18] (b) **2H7M**,[22] (c) **3FNE**,[20] (d) **2B37**,[19] (e) **1LXC**.[40] The volume depicted in (f) delineates the accessible region occupied by the inhibitors into the binding pocket. It results from the overlay of 14 InhA inhibitors found in the Protein Data Bank.

Table 2 Calculated interaction energies (kcal mol^{-1}) of the first ranked Autodock Vina pose and the most relevant conformation when different from the first Autodock Vina pose[a]

		Autodock Vina			MOPAC (PM6-DH2)		
Ligand	Protein code	E_{Vina} (rank)	RMSD (Å)	H-bonds with Y158/ribose	Single point E_{sp} (rank)	Optimization E_{opt} (rank)	Position compared with the X-ray ligand
GEQ	***1P44***	*−10.9 (1)*	*0.3*	*2*	*−21.1 (1)*	*−60.8 (1)*	*Correct*
	1P45	−9.2 (1)	8.2	1	17.4 (10)	−22.1 (5)	Inverted
		−7.9 (10)	2.0	2	3.9 (5)	−42.5 (1)	Fluorene flipped
	2H7M	−8.3 (1)	1.9	2	−33.4 (1)	−42.5 (1)	Correct
	3FNE	−8.8 (1)	8.5	—	0.3 (9)	−23.3 (5)	Inverted
		−7.9 (3)	3.6	1	−20.4 (1)	−25.6 (4)	Shifted
d11	**1P44**	−7.5 (1)	5.8	—	−2.1 (3)	−14.1 (2)	Improper
		−7.3 (3)	1.1	2	−2.7 (1)	−24.9 (1)	Correct
	1P45	−7.9 (1)	7.0	—	−8.5 (1)	−5.3 (8)	Inverted, folded
		−7.2 (2)	2.9	2	−2.3 (2)	−19.3 (3)	Amide flipped
	2H7M	*−8.3 (1)*	*0.4*	*2*	*−15.0 (1)*	*−37.5 (2)*	*Correct*
	3FNE	−7.7 (1)	10.7	—	10.2 (10)	−3.6 (10)	Out
		−7.4 (2)	2.3	2	−12.2 (1)	−17.6 (2)	Aryl displaced
8PC	**1P44**	−5.5 (1)	3.3	—	−6.6 (3)	+1.0 (7)	Shifted
		−5.4 (2)	1.6	2	−16.6 (1)	−19.1 (3)	Correct
	1P45	−6.0 (1)	1.1	2	−7.8 (1)	−25.3 (1)	Correct
	2H7M	−7.6 (1)	7.7	2	4.8 (4)	−16.7 (5)	Inverted
		−7.5 (2)	1.7	3	−11.2 (1)	−17.8 (3)	Correct
	3FNE	*−6.6 (1)*	*0.5*	*2*	*−11.5 (1)*	*−25.4 (1)*	*Correct*
8PS	**1P44**	−3.9 (1)	8.0	—	−7.3 (8)	−12.8 (9)	Inverted
		−3.8 (2)	2.4	2	−9.3 (6)	−29.3 (1)	Slightly shifted
	1P45	−5.2 (1)	2.9	2	−30.1 (1)	−31.3 (1)	Correct
	2H7M	−5.4 (1)	2.7	2	−27.5 (1)	−34.5 (1)	Correct
	3FNE	−7.2 (1)	3.7	—	−20.2 (2)	−24.5 (2)	Shifted
		−7.1 (2)	2.1	3	−26.5 (1)	−45.7 (1)	Correct
AYM	**1P44**	−7.7 (1)	4.8	—	−7.17 (3)	−25.3 (4)	Improper
		−6.9 (8)	2.7	1	−14.6 (1)	−30.5 (2)	Shifted, indole flipped
	1P45	−8.0 (1)	7.7	—	20.2 (9)	−6.9 (7)	Inverted
		−7.7 (2)	1.0	2	−7.5 (1)	−32.2 (4)	Correct
	2H7M	−7.8 (1)	1.4	2	−20.1 (1)	−38.2 (1)	Correct
	3FNE	−7.4 (1)	10.7	—	−6.9 (2)	−14.5 (3)	Partly out
		−6.9 (3)	2.4	1	−18.0 (1)	−33.0 (1)	Shifted

[a] Italic fonts correspond to calculations performed with the ligands docked in their respective InhA native proteins. *Inverted* pose is relative to a conformation that is inverted compared to the crystal structure of reference. The *out* or *partly out* poses were docked outside the acyl substrate-binding pocket. The computed volume occupied by 14 inhibitors was used to evaluate this "out-of-cavity" notion. The *improper* poses refer to other docked pose whose orientation was far from the awaited result. *Shifted, flipped*, *folded*, *displaced* poses are relative to conformations that are oriented in the same way as in the crystal structure of reference, but with some minor changes.

3FNE, Table 2, lines in italic). The corresponding RMSD were small (0.3, 0.4 and 0.5 Å) and moreover, the PM6-DH2 optimizations gave also the best energetic scores (E_{opt} = −60.8, 37.5 and −25.4 kcal mol^{-1}).

In this multiple receptor docking approach, we can also bring out that the **2H7M** cavity appeared as a highly versatile enzyme to dock the direct inhibitors of InhA. Indeed, all the crystallographic conformations of inhibitors could be retrieved with this unique enzyme and in all cases, the first or second Vina model as well as the best score obtained by PM6-DH2 corresponded to the correct conformation of the ligand in the native enzyme (Table 2).

Some specific comments for each ligand are presented hereafter.

Docking of GEQ

GEQ refers to the ligand found in the **1P44** entry. This compound is characterized by its bulky size and a rigidity imposed by the polycyclic framework. The carbonyl group of **GEQ** is hydrogen-bonded to the 2′-hydroxyl of the nicotinamide ribose and to Y158 (Fig. 1a). At the opposite part of the molecule, the fluorene moiety is located in a hydrophobic pocket. In the X-ray data, the piperazine ring is in a twisted conformation which imposes the orientation of the fluorene and indoyl moieties. We kept this geometry thereafter.

As specified above, using the **2H7M** cavity, the Vina first binding mode fitted well with the bioactive conformation (RMSD = 1.9 Å). With the two other proteins (**1P45** and **3FNE**), the correct positioning of the bulky fluorene group into the hydrophobic pocket was hindered by the L218, A157 and M199 side chains. Consequently, in both proteins, the two top-ranked poses found by Vina were in an inverted orientation compared to the expected crystal structure (Fig. S1† in Online Resource). Moreover, in **3FNE**, half of docked models were rejected out of the ligand cavity. The most relevant result (Vina model 3) was rather shifted. The positioning could not be improved due to the hindrances and the MOPAC minimization classified this at only the fourth position. In **1P45**, the most

correct orientation corresponded to the Vina tenth binding mode (RMSD = 2.0 Å) characterized by a flipped fluorene group and the presence of the two expected H-bonds with the carbonyl oxygen. The PM6-DH2 full optimization gave the best energetic score for this conformation (E_{opt} = −42.5 kcal mol^{-1}) which could consequently be selected.

Fig. 2a shows the superimposition of the best result found with **GEQ** for each protein.

Docking of d11

The cyclohexyl-pyrrolidinone carboxamide derivative **d11** was co-crystallized in **2H7M**. In **2H7M** crystal, the carbonyl of the pyrrolidinone moiety is involved in an hydrogen-bonding network with Y158 and the 2′-hydroxyl ribose while the dichlorophenyl group is located in the same hydrophobic region as the fluorene group of **GEQ** in **1P44** (Fig. 1b).

With **1P44**, Vina models 1 and 2 showed an inappropriate folded conformation far from the crystallographic structure; furthermore their RMSD values were superior to 5 Å. On the other hand, model 3 was very close to the structure found in **2H7M** and the expected H-bond network was observable (RSMD = 1.5 Å). The PM6-DH2 optimization step allowed to select the correct model 3 (E_{opt} = −14.1, −12.1 and −24.9 kcal mol^{-1} for models 1, 2 and 3, respectively).

With **3FNE**, only Vina models 2, 4 and 6 were entirely located into the binding pocket; the other poses were partially out-of-cavity. Model 2 was the most properly positioned (RMSD = 2.3 Å). Due to unfavourable interactions with L218 and M199, the dichlorophenyl moiety was displaced, but the expected H-bond network could be observed. Both MOPAC PM6-DH2 single point and minimization gave the best score for this latter (E_{sp} = −12.2 kcal mol^{-1} and E_{opt} = −17.6 kcal mol^{-1}).

The **1P45** results were less obvious. Vina model 2 exhibited the two critical H-bonds but, in order to minimize the steric interactions with A157 and L218, the dichlorophenyl amide group rotated at 180°, leading to a higher RMSD (2.9 Å). The PM6-DH2 optimization ranked it at the third position (E_{opt} = −19.3 kcal mol^{-1}). The model 5 was predicted by the PM6-DH2 optimization (E_{opt} = −25.1 kcal mol^{-1}) as the best one but this latter was in an inverted orientation and did not exhibit any relevant interaction.

Finally, beside the **2H7M** reference cavity, the expected conformation of **d11** was successfully found with **1P44** and to a lesser extent with **3FNE**. With **1P45**, only partially correct conformations of **d11** could be detected. Fig. 2b shows superimposition of the best docked conformation of **d11** for each protein.

Docking of 8PC

The pyridine methyl substituted TCL derivative **8PC** is found in the PDB entry **3FNE**. It interacts in the same way as TCL. These two ligands are perfectly superimposable when the corresponding proteins **3FNE** and **1P45** are fitted. The phenolic oxygen is oriented in the same manner as the carbonyl oxygen of the other ligands (**GEQ**, **d11** and **AYM**) and forms a three hydrogen-bonding pattern with Y158 and NADH (Fig. 1c).

Autodock Vina readily found the crystallographic conformation of **8PC** in the **1P45** cavity (RMSD = 1.1 Å) with the

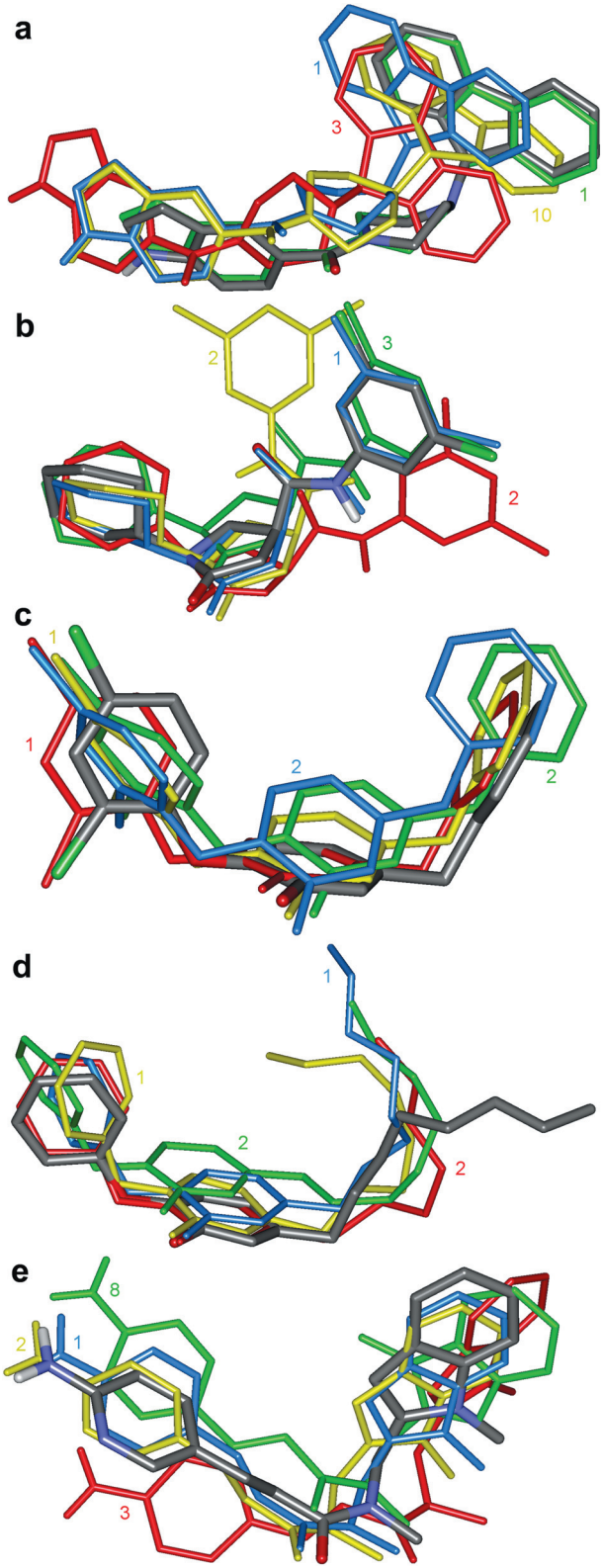

Fig. 2 Superimposition of the most relevant docked structures of **GEQ** (a), **d11** (b), **8PC** (c), **8PS** (d) **AYM** (e) for each protein. The experimental conformations of the ligands found in the X-ray structures are in a CPK-coloured representation. Conformations relative to **1P44**, **1P45**, **2H7M** and **3FNE** are depicted in green, yellow, blue, and red, respectively. The numbers in the figure correspond to the Vina ranking.

top-ranked pose. The PM6-DH2 optimization gave also the best energetic score (E_{opt} = −25.3 kcal mol^{-1}). The model 1 found in **2H7M** proved to be in an inverted orientation, with E_{opt} = −16.7 kcal mol^{-1}, whereas the second one showed a correct orientation (RMSD = 1.7 Å) and exhibited a better interaction energy (E_{opt} = −17.8 kcal mol^{-1}). These two poses were the only that showed a H-bond network with Y158 and 2′-hydroxyl of nicotinamide ribose.

With **1P44**, Vina model 2 was appropriate (RMSD = 1.6 Å); the E_{opt} value (−19.1 kcal mol^{-1}) ranked it in third position; Vina model 5 (−23.6 kcal mol^{-1}) or model 4 (−24.8 kcal mol^{-1}) had a better E_{opt} score. Both exhibited an appropriate H-bond network but were in inverted or shifted positions.

Thus, the expected conformation of **8PC** could be successfully found with **1P45** and **2H7M**. The most appropriate conformations of **8PC** are shown in Fig. 2c.

Docking of 8PS

The compound **8PS** is a non-chlorinated TCL derivative substituted by a C_8 alkyl chain designed to mimic the acyl substrate chain.[19] It was co-crystallized with InhA (PDB entry 2B37) (Fig. 1d). Among all the ligands, it was probably the most challenging compound submitted to Autodock Vina insofar as 25 rotatable bonds (15 of which into the protein) were set. Vina did not find the complete alkyl chain location into the cavities, but it was able to properly orient the phenoxyphenol moiety and the first part of the alkyl chain. This chain being a source of flexibility, the RMSD values were slightly higher compared to other ligands.

The **3FNE** cavity gave an accurate docking result with both Vina models 1 and 2. However with Vina model 2, a favourable RMSD value of 2.1 Å was obtained with the phenoxyphenol moiety fitting well with the crystallographic coordinates and the C_8 alkyl chain being oriented correctly. Moreover, the interaction energies calculated with this model (E_{sp} = −26.5 kcal mol^{-1}; E_{opt} = −45.7 kcal mol^{-1}) were unambiguously the lowest ones.

Autodock Vina succeeded also in finding very relevant poses with the three other proteins. The poses 1 and 2 were the most appropriate for **1P45**. All the other results were shifted or in a wrong position. Both E_{sp} and E_{opt} calculated interaction energies enabled to select in the first place the model 1 (E_{sp} = −30.1 kcal mol^{-1}; E_{opt} = −31.3 kcal mol^{-1}).

Only the second pose found with **1P44** was correct (RMSD = 2.4 Å) and displayed the awaited H-bond network with Y158 and the 2′-hydroxyl of the nicotinamide ribose. The PM6-DH2 full minimization allowed to choose this one without ambiguity (E_{opt} = −29.3 kcal mol^{-1}).

In summary, Vina was able to find the correct interaction of **8PS** in the four protein cavities and the PM6-DH2 optimization led to an improvement of the docking and allowed to select unequivocally the proper positioning in all the proteins. The best docked conformations of **8PS** are shown in Fig. 2d.

Docking of AYM

The aminopyridine derivative **AYM** was co-crystallized with the *E. coli* enoyl-ACP reductase 1LXC (FabI).[40] **AYM** interacts in **1LXC** in the same manner as other ligands do with InhA: the carbonyl is involved in a H-bond network with the 2′-hydroxyl of nicotinamide ribose and the phenolic hydroxyl of Y156, the amino acid homologue of the InhA Y158. A third H-bond is found between A95 and the pyridine nitrogen. In InhA, the amino acid homologue of A95 is M98.

Vina model 2 in **1P45** as well as Vina model 1 in **2H7M** were very well-docked with RMSD of 1.0 and 1.4 Å respectively. MOPAC single point calculations allowed the selection of these conformations as the good ones and the PM6-DH2 optimization was able to improve the ligands positioning: the two expected H-bonds were found and, interestingly, two supplementary H-bonds were observed between the aminopyridine group and the M98 residue (Fig. S2† in Online Resource).

In **1P44**, the model 8 was the most relevant (RMSD = 2); it was correctly oriented although shifted and had its indolyl moiety rotated at 180°.

In **3FNE**, only model 3 was properly docked, although shifted. One H-bond was observable between the carbonyl group and the hydroxyl of Y158. All the other poses were in some extent outside the cavity. The PM6-DH2 optimization led to a displacement of the ligand which improved the docking (the RMSD value diminished from 2.4 to 2.0 Å) and a second H-bond interaction with the 2′-hydroxyl of nicotinamide ribose was found (Fig. S3† in Online Resource).

As a conclusion, Vina efficiently docked **AYM** in **1P45** and **2H7M**. In **3FNE** and **1P44**, the best poses were less accurate but were improved by a MOPAC optimization and remained acceptable, particularly with **3FNE**. The best docked conformations of **AYM** are shown in Fig. 2e.

Discussion

Several methodologies have been proposed in recent years to incorporate protein flexibility into the docking process.[27,29–32] In the ensemble-docking, multiple receptor conformations are used to describe protein flexibility. This approach is relatively fast and is known to improve docking calculations as the receptor conformations are carefully chosen.[30] We applied this approach to four available InhA crystallographic structures using Autodock Vina. This software allowed us to consider the motions of the side chains surrounding the cavities and therefore to better explore the available space into the cavity. It proved to be very fast and very efficient in retrieving the crystallographic conformations of the studied ligands.

But in several cases, the correct geometries were not well classified by Autodock Vina alone. This could generally be explained by the hindrance generated by some bulky or flexible amino-acid residues (*i.e.* M199, L218, A157…) whose side chains exhibited a wide amplitude of motion and were differently oriented according to the cavity. The use of the MOPAC PM6-DH2 routine in a post-docking optimization proved to be very efficient to locate these improperly classified Vina poses. This semi-empirical method allowed to consider with a good accuracy and an acceptable speed of execution, the electronic and polarization effects induced by the protein environment. We could verify that in many cases, the optimization of both the inhibitors and twelve amino acid side chains delimiting the binding pocket

improved the positioning of the ligands into the cavities and allowed the apparition of relevant interactions. With the resulting interaction energies, we were able to retrieve the bioactive conformation of each ligand.

Some wrong predictions were nevertheless obtained where E_{sp} or E_{opt} failed to select the proper results. As examples, wrong predictions by using E_{sp} values were obtained: with **GEQ**/**1P45**, the wrong poses 3, 8 and 9 were better ranked than the more appropriate pose 10 (Table S3,† Online Resource); with **d11**/**1P45**, the model 1 which was in an inverted position would be chosen instead of the correct pose 2. As other examples, the E_{opt} criterion failed to differentiate the proper result for some docking poses which were in inverted orientation but exhibited relevant interactions (**GEQ** pose 2 in **3FNE**, **d11** pose 5 in **1P45**, **AYM** pose 8 in **1P45**).

These failures underline the interest to use the ensemble docking approach, since the correct ligand binding modes finally could be retrieved, as commented hereafter.

As the bioactive conformations were logically found when the ligands were docked into their native protein, only data obtained for ligands in interaction with non-native proteins will be taken in consideration in the following discussion, that represents 17 ligand/protein analyses (Table 3). With the five inhibitors used in this study, the top-ranked Vina pose corresponded to the suitable conformation in only 5 cases out of 17 (Tables 3 and 4).

However, we must note that the bioactive conformation could be found with almost all the proteins either in the first, the second or the third Vina model excepted in two cases (**GEQ** in interaction with **1P45**, and **AYM** in interaction with **1P44**). Furthermore, calculation of E_{sp} or E_{opt} interaction energies used as scoring methods on the 3 top-ranked Vina models allows selection of the more suitable poses in 13 out of 17 cases, and, when combining both the 3 best Vina poses and both E_{sp} and E_{opt} scores, 15 out of 17 cases (Table 4). Considering each ligand separately, this last predictive model allows to retrieve the bioactive conformations in 2 out of 3 cases (**GEQ**), 3 out of 3 cases (**d11** and **8PC**), 4 out of 4 cases (**8PS**) and 3 out of 4 cases (**AYM**).

Table 3 Vina ranks corresponding to the correct binding modes for each InhA[a]

	Ligand					
InhA	**GEQ**	**d11**	**8PC**	**8PS**	**AYM**	Vina rank 1 success rate
1P44	*1*	3	2	2	8	0/4
1P45	10	2	1	1	2	2/5
2H7M	1	*1*	2	1	1	3/4
3FNE	3	2	*1*	2	3	0/4

[a] Italic fonts correspond to the ligand docked into its native protein; these results are not included into the "success rate" column.

Table 4 Rate of correct prediction for each ligand using: the first Vina model, the 3 first Vina models combined with E_{sp}, or E_{opt}, or both E_{sp} and E_{opt} Mopac energetic values

	Correct success rate of prediction					Overall success rate
	GEQ	**d11**	**8PC**	**8PS**	**AYM**	
Vina model 1	1/3	0/3	1/3	2/4	1/4	5/17
Vina models 1,2,3 + E_{sp}	2/3	2/3	3/3	3/4	3/4	13/17
Vina models 1,2,3 + E_{opt}	1/3	3/3	3/3	4/4	2/4	13/17
Vina models 1,2,3 + E_{sp} + E_{opt}	2/3	3/3	3/3	4/4	3/4	15/17

Table 5 Computed volume of binding pockets

InhA	**1P44**	**1P45**	**2H7M**	**3FNE**
Volume (Å^3)	907	896	849	689

The results obtained with **3FNE** need some additional comments. Except for **8PC** and **8PS**, Autodock Vina gave less accurate results for other ligands and poses were frequently found out of the cavity. We computed the volume of each protein cavity with the VOIDOO Package.[55] These values are given in Table 5 and show that the **3FNE** binding pocket is the narrowest. Thus, the particular docking results obtained with the **3FNE** cavity may probably be explained by its smaller size compared to the others.

One other point to discuss is the use of our method to predict the affinity of the ligands towards InhA. Table 2 shows that the calculated interaction energies differ widely for a given compound depending on the used target. These fluctuations reflect essentially the constraints imposed during the minimizations: only twelve amino acid side chains were allowed to move, the other ones as well as the protein backbone were kept frozen. This forced rigidity might sometimes hinder a better positioning of the ligand into the cavity. The increase of the degrees of freedom into the protein (*i.e.* more moving residues) would probably be beneficial but are more time-consuming. One can notice that for a given ligand, the best result obtained with MOPAC was for the co-crystallized ligand/receptor pairs (**GEQ**/**1P44**, **d11**/**2H7M** and **8PC**/**3FNE**) which corresponds to the optimal interactions. Among the compounds tested as inhibitors of InhA, the TCL derivatives **8PC** and **8PS** were described as potent inhibitors,[19,20] with nanomolar activities (IC_{50} = 29 and 5 nM, respectively, Table 1) whereas **GEQ** was one of the less active of this series,[18] with a IC_{50} value of 0.16 μM. Surprisingly, both the Vina and PM6-DH2 scores gave **GEQ** as the best inhibitor (E_{vina} = −10.9 and E_{opt} = −60.8 kcal mol^{-1}) while the energies were −6.6 and −25.4 kcal mol^{-1}, respectively, for **8PC** and −7.1 and −45.7 kcal mol^{-1}, respectively, for **8PS**. No real correlations could in fact be done between the experimental and the calculated results neither with Vina nor with Mopac. The few number of molecules as well as their structural diversity make this analysis rather delicate. The apparent overestimated score found with **GEQ** might be due in part to differences in the experimental conditions in the determination of the IC_{50} values. Besides, we did consider neither the entropy terms nor the energy of solvation in the energy calculations. In order to optimize the design of a new series of InhA inhibitors,[38] we will include these latter aspects, using the linear response methods.[56,57]

Conclusion

In the present article, the Autodock Vina docking software was used in an ensemble docking procedure in combination with

post-docking PM6-DH2 MOPAC energy calculations. The enoyl-ACP reductase InhA, a key enzyme from *Mycobacterium tuberculosis* which is an attractive target for the development of new antitubercular agents, was used as receptor. In order to consider receptor flexibility, four InhA crystal structures were used. Five InhA inhibitors for which the bioactive conformations are known were sequentially docked in each InhA cavity. The accuracy of this approach was estimated by comparing the predicted binding modes of the InhA inhibitors with their crystallographic structure found in complex with InhA. Autodock Vina proved fast and rather efficient in predicting models near the crystal structures. The bioactive conformation was not systematically top ranked by the Vina scoring function but could be generally ranked in the three first positions. Post-docking PM6-DH2 interaction energy calculations allowed then to select the correct ligand binding mode. For each ligand studied, the use of the multiple receptor conformations approach allowed to select very relevant conformations with RMSD values ≤2.0 Å, compared to the crystal structure. This strategy will subsequently be applied in the optimization of a new series of InhA inhibitors.

Notes and references

1 R. F. Waller, P. J. Keeling, R. G. Donald, B. Striepen, E. Handman, N. Lang-Unnasch, A. F. Cowman, G. S. Besra, D. S. Roos and G. I. McFadden, *Proc. Natl. Acad. Sci. U. S. A.*, 1998, **95**, 12352–12357.
2 A. Quemard, J. C. Sacchettini, A. Dessen, C. Vilcheze, R. Bittman, W. R. J. Jacobs and J. S. Blanchard, *Biochemistry*, 1995, **34**, 8235–8241.
3 A. Dessen, A. Quemard, J. S. Blanchard, W. R. Jacobs and J. C. Sacchettini, *Science*, 1995, **267**, 1638–1641.
4 A. Banerjee, E. Dubnau, A. Quemard, V. Balasubramanian, K. S. Um, T. Wilson, D. Collins, G. de Lisle and W. R. J. Jacobs, *Science*, 1994, **263**, 227–230.
5 K. Bartmann, H. Iwainsky, H. H. Kleeberg, P. Mison, H. A. Offe, H. Otten, D. Tettenborn and L. Trnka, *Antituberculosis Drugs*, Springer-Verlag, 1988.
6 K. Johnsson and P. G. Schultz, *J. Am. Chem. Soc.*, 1994, **116**, 7425–7426.
7 J. C. Sacchettini and J. S. Blanchard, *Res. Microbiol.*, 1996, **147**, 36–43.
8 D. A. Rozwarski, G. A. Grant, D. H. Barton, W. R. J. Jacobs and J. C. Sacchettini, *Science*, 1998, **279**, 98–102.
9 A. Quemard, A. Dessen, M. Sugantino, W. R. Jacobs, J. C. Sacchettini and J. S. Blanchard, *J. Am. Chem. Soc.*, 1996, **118**, 1561–1562.
10 R. Rawat, A. Whitty and P. J. Tonge, *Proc. Natl. Acad. Sci. U. S. A.*, 2003, **100**, 13881–13886.
11 B. Lei, C. J. Wei and S. C. Tu, *J. Biol. Chem.*, 2000, **275**, 2520–2526.
12 R. J. Heath, J. Li, G. E. Roland and C. O. Rock, *J. Biol. Chem.*, 2000, **275**, 4654–4659.
13 R. J. Heath and C. O. Rock, *Nature*, 2000, **406**, 145–146.
14 R. J. Heath, N. Su, C. K. Murphy and C. O. Rock, *J. Biol. Chem.*, 2000, **275**, 40128–40133.
15 R. J. Heath, Y. T. Yu, M. A. Shapiro, E. Olson and C. O. Rock, *J. Biol. Chem.*, 1998, **273**, 30316–30320.
16 L. M. McMurry, P. F. McDermott and S. B. Levy, *J. Antimicrob. Chemother.*, 1999, **43**, 711–713.
17 S. L. Parikh, G. Xiao and P. J. Tonge, *Biochemistry*, 2000, **39**, 7645–7650.
18 M. R. Kuo, H. R. Morbidoni, D. Alland, S. F. Sneddon, B. B. Gourlie, M. M. Staveski, M. Leonard, J. S. Gregory, A. D. Janjigian, C. Yee, J. M. Musser, B. Kreiswirth, H. Iwamoto, R. Perozzo, W. R. Jacobs, J. C. Sacchettini and D. A. Fidock, *J. Biol. Chem.*, 2003, **278**, 20851–20859.
19 T. J. Sullivan, J. J. Truglio, M. E. Boyne, P. Novichenok, X. Zhang, C. F. Stratton, H. Li, T. Kaur, A. Amin, F. Johnson, R. A. Slayden, C. Kisker and P. J. Tonge, *ACS Chem. Biol.*, 2006, **1**, 43–53.
20 J. S. Freundlich, F. Wang, C. Vilcheze, G. Gulten, R. Langley, G. A. Schiehser, D. R. Jacobus, W. R. Jacobs and J. C. Sacchettini, *ChemMedChem*, 2009, **4**, 241–248.
21 X. He, A. Alian and P. R. Ortiz de Montellano, *Bioorg. Med. Chem.*, 2007, **15**, 6649–6658.
22 X. He, A. Alian, R. Stroud and P. R. Ortiz de Montellano, *J. Med. Chem.*, 2006, **49**, 6308–6323.
23 S. Broussy, V. Bernardes-Génisson, H. Gornitzka, J. Bernadou and B. Meunier, *Org. Biomol. Chem.*, 2005, **3**, 666–669.
24 S. Broussy, V. Bernardes-Génisson, A. Quemard, B. Meunier and J. Bernadou, *J. Org. Chem.*, 2005, **70**, 10502–10510.
25 T. Delaine, V. Bernardes-Génisson, B. Meunier and J. Bernadou, *J. Org. Chem.*, 2007, **72**, 675–678.
26 T. Delaine, V. Bernardes-Génisson, A. Quémard, P. Constant, B. Meunier and J. Bernadou, *Eur. J. Med. Chem.*, 2010, **45**, 4554–4561.
27 C. B-Rao, J. Subramanian and S. D. Sharma, *Drug Discovery Today*, 2009, **14**, 394–400.
28 P. Cozzini, G. E. Kellogg, F. Spyrakis, D. J. Abraham, G. Costantino, A. Emerson, F. Fanelli, H. Gohlke, L. A. Kuhn, G. M. Morris, M. Orozco, T. A. Pertinhez, M. Rizzi and C. A. Sotriffer, *J. Med. Chem.*, 2008, **51**, 6237–6255.
29 M. L. Teodoro and L. E. Kavraki, *Curr. Pharm. Des.*, 2003, **9**, 1635–1648.
30 M. Totrov and R. Abagyan, *Curr. Opin. Struct. Biol.*, 2008, **18**, 178–184.
31 S. B. Nabuurs, M. Wagener and J. de Vlieg, *J. Med. Chem.*, 2007, **50**, 6507–6518.
32 H. Alonso, A. A. Bliznyuk and J. E. Gready, *Med. Res. Rev.*, 2006, **26**, 531–568.
33 X. Barril and S. D. Morley, *J. Med. Chem.*, 2005, **48**, 4432–4443.
34 S. Huang and X. Zou, *Proteins: Struct., Funct., Bioinf.*, 2007, **66**, 399–421.
35 O. Trott and A. J. Olson, *J. Comput. Chem.*, 2010, **31**, 455–461.
36 J. J. P. Stewart, *J. Mol. Model.*, 2007, **13**, 1173–1213.
37 J. Rezac, J. Fanfrlik, D. Salahub and P. Hobza, *J. Chem. Theory Comput.*, 2009, **5**, 1749–1760.
38 C. Deraeve, I. M. Dorobantu, F. Rebbah, F. Le Quéméner, P. Constant, A. Quémard, V. Bernardes-Génisson, J. Bernadou and G. Pratviel, *Bioorg. Med. Chem.*, 2011, **19**, 6225–6232.
39 H. M. Berman, J. Westbrook, Z. Feng, G. Gilliland, T. N. Bhat, H. Weissig, I. N. Shindyalov and P. E. Bourne, *Nucleic Acids Res.*, 2000, **28**, 235–242.
40 W. H. Miller, M. A. Seefeld, K. A. Newlander, I. N. Uzinskas, W. J. Burgess, D. A. Heerding, C. C. K. Yuan, M. S. Head, D. J. Payne, S. F. Rittenhouse, T. D. Moore, S. C. Pearson, V. Berry, W. E. DeWolf, P. M. Keller, B. J. Polizzi, X. Qiu, C. A. Janson and W. F. Huffman, *J. Med. Chem.*, 2002, **45**, 3246–3256.
41 V. B. Chen, W. B. I. Arendall, J. J. Headd, D. A. Keedy, R. M. Immormino, G. J. Kapral, L. W. Murray, J. S. Richardson and D. C. Richardson, *Acta Crystallogr., Sect. D: Biol. Crystallogr.*, 2010, **66**, 12–21.
42 R. Harrison, *J. Comput. Chem.*, 1993, **14**, 1112–1122.
43 A. Pedretti, L. Villa and G. Vistoli, *J. Comput.-Aided Mol. Des.*, 2004, **18**, 167–173.
44 J. J. P. Stewart, *Stewart Computational Chemistry*, Colorado Springs, CO, USA, http://OpenMOPAC.net
45 M. W. Chang, C. Ayeni, S. Breuer and B. E. Torbett, *PLoS One*, 2010, **5**, e11955.
46 M. F. Sanner, B. S. Duncan, C. J. Carrillo and A. J. Olson, *Pac. Symp. Biocomput.*, 1999, **4**, 401–412.
47 G. M. Morris, R. Huey, W. Lindstrom, M. F. Sanner, R. K. Belew, D. S. Goodsell and A. J. Olson, *J. Comput. Chem.*, 2009, **30**, 2785–2791.
48 E. Perola, W. P. Walters and P. S. Charifson, *Proteins: Struct., Funct., Bioinf.*, 2004, **56**, 235–249.
49 J. Koska, V. Z. Spassov, A. J. Maynard, L. Yan, N. Austin, P. K. Flook and C. M. Venkatachalam, *J. Chem. Inf. Model.*, 2008, **48**, 1965–1973.
50 J. Stigliani, P. Arnaud, T. Delaine, V. Bernardes-Génisson, B. Meunier and J. Bernadou, *J. Mol. Graphics Modell.*, 2008, **27**, 536–545.
51 J. J. P. Stewart, *Int. J. Quantum Chem.*, 1996, **58**, 133–146.
52 A. Klamt and G. Schuurmann, *J. Chem. Soc., Perkin Trans. 2*, 1993, 799–805.
53 M. Korth, M. Pitonak, J. Rezac and P. Hobza, *J. Chem. Theory Comput.*, 2010, **6**, 344–352.
54 Accelrys, Inc., 10188 Telesis Court, Suite 100, San Diego, CA 92121, USA.
55 G. J. Kleywegt and T. A. Jones, *Acta Crystallogr., Sect. D: Biol. Crystallogr.*, 1994, **50**, 178–185.
56 J. Åqvist, C. Medina and J. E. Samuelsson, *Protein Eng., Des. Sel.*, 1994, **7**, 385–391.
57 T. Hansson, J. Marelius and J. Åqvist, *J. Comput.-Aided Mol. Des.*, 1998, **12**, 27–35.